HATSOPOULOS MICROFLUIDS LABORATORY
Department of Mechanical Engineering, Massachusetts Institute of Technology

Controlling the Location and Spatial Extent of Nanobubbles Using Hydrophobically Nanopatterned Surfaces

Abhinandan Agrawal, Juhyun Park, Du. Y. Ryu, Paula T. Hammond, Thomas P. Russell, and Gareth H. McKinley

August 5, 2005
HML Report Number 05-P-09

HML@MIT
http://web.mit.edu/fluids

Controlling the location and spatial extent of nanobubbles using hydrophobically nanopatterned surfaces

Abhinandan Agrawal,[⊥] *Juhyun Park,*[┼] *Du Y. Ryu,*[‖] *Paula T. Hammond,*[¶] *Thomas P. Russell,*[‖] *and Gareth H. McKinley*[*,⊥]

Hatsopoulos Microfluids Laboratory, Department of Mechanical Engineering, Department of Material Science and Engineering, Department of Chemical Engineering, Massachusetts Institute of Technology, Cambridge, Massachusetts 02139, and Polymer Science and Engineering Department, University of Massachusetts, Amherst, Massachusetts 01003

[*] Corresponding author. E-mail: gareth@mit.edu. Tel.: 617-258-0754. Fax: 617-258-8559.

[⊥] Hatsopoulos Microfluids Laboratory, Department of Mechanical Engineering, Massachusetts Institute of Technology.

[┼] Department of Material Science and Engineering, Massachusetts Institute of Technology.

[‖] Polymer Science and Engineering Department, University of Massachusetts.

[¶] Department of Chemical Engineering, Massachusetts Institute of Technology.

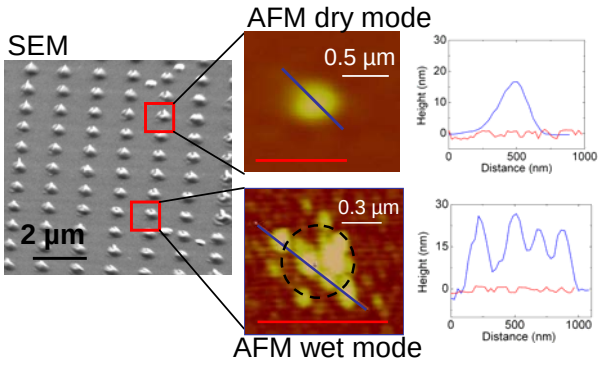

ABSTRACT: The presence of nanobubbles—as imaged with tapping-mode atomic force microscopy—is controlled using nanopatterned surfaces possessing repeating patterns of polystyrene (hydrophobic domains) and polymethyl-methacrylate (hydrophilic domains). For nanobubbles to be present, we find that, in addition to controlling the degree of surface hydrophobicity, it is important for the spatial dimensions of the hydrophobic domains on the nanopatterned surface to be commensurate with the equilibrium topology of the nanobubbles.

Nanobubbles, with 5–100 nm heights and 0.1–0.8 µm diameters, are found to appear spontaneously at the interface between a polar solvent (e.g. water) saturated with air and hydrophobic surfaces.[1-8] The presence of these bubbles has been detected by atomic force microscopy,[1-3, 5, 7, 8] as well as other techniques including rapid cyrofixation/freeze fracture and neutron reflectometry.[4, 6] Although the origin of these bubbles is unclear and some debate remains in the literature about their existence,[9, 10] they have recently been invoked as a possible origin of number of phenomena, including, the long-range attraction between hydrophobic surfaces immersed in water,[10, 11] the stability of an emulsion without a surfactant,[12] microboiling behavior,[13] mineral flotation,[14] and the rupture of wetting films.[15] Nanobubbles on surfaces can also have significant consequences on the motion of particles in liquids or on the flow of liquids adjacent to surfaces or in capillaries. We can expect a reduction in drag by such nanobubbles, since interfacial slip obviously occurs at a fluid-fluid interface, whereas no-slip boundary conditions are traditionally expected in hydrodynamic flows bounded by solid surfaces. It has also been

argued that nanobubbles lead to the frequency-dependent and shear-rate dependent fluid-slip that has been recently observed at partially wetting fluid-solid surfaces,[16-18] and which gives rise to considerable reduction in friction of fluid flow past the solids. From the earlier publications it can be concluded that formation of nanobubbles strongly depends on the properties of the substrates. While they exist primarily on hydrophobic surfaces, they do not appear spontaneously on hydrophilic surfaces, unless they form from the differences in the solubility of air between two miscible fluids.[19-22]

Nanobubbles offer an effective mechanism for drag reduction in microfluidic applications, in which interfacial properties are expected to dominate the dynamics due to the large surface to volume ratio.[23] The aim of this study is to exploit the dependence of nanobubble formation on surface hydrophobicity to provide a means for controlling hydrodynamic boundary conditions at the solid-liquid interface. We have used patterned surfaces with nanometer length scale domains of varying hydrophobicity in order to manipulate the formation and extent of nanobubbles. To the best of our knowledge, this is the first experimental study in which chemically inhomogeneous surfaces are used to probe the existence of nanobubbles. We note that the concerted effect of nanoscale patterns and chemical hydrophobicity, which is used in this study to control the presence of nanobubbles, has also been recently shown to have an important effect on macroscopic wetting phenomena.[24, 25]

We present results from experiments with different homogenous as well as nanopatterned surfaces. A Nanoscope IV MultiMode atomic force microscope (AFM) was used in tapping- as well as contact-mode to image the solid-liquid interface. Homogenous polymethyl-methacrylate (PMMA) and polystyrene (PS) surfaces, prepared by spin-coating, were first used to investigate the difference in the formation of nanobubbles on homogenous surfaces with different hydrophobicities. We then extend our study to three sets of nanopatterned surfaces. Block copolymer self-assembly[26, 27] as well as polymer transfer printing[28, 29] were used to prepare the patterned polymer surfaces. In conjunction with surface hydrophobicity, the lateral dimensions of the hydrophobic regions were also found to be important in

governing the presence of nanobubbles. The methods of surface preparation along with other experimental details are discussed in the Supporting Information.

First, we discuss results with homogenous PMMA surfaces. Smooth spincoated surfaces are found to give a contact angle value of ~72^{o} with water, which suggests that PMMA surfaces are partially wetting in nature.[30] Figure 1A shows the contact-mode AFM height image of a PMMA surface in air. The image is featureless and reveals no spatial structure. Two parameters are defined henceforth to provide quantitative measures of the level of surface roughness in an image. Firstly, we define the root-mean-square roughness (R)[31] as

$$R = \sqrt{\frac{\sum_{i=1}^{N}\sum_{j=1}^{N} Z^2(x_i, y_j)}{N^2}}$$

Z is the height deviation taken from the mean image data plane; N is the number of data points in one scan direction. The second parameter is R_{max} ; it is defined as the vertical distance between the highest and lowest data points in an image. For the image in Figure 1A, R = 0.27 nm and R_{max} = 2.2 nm. Figure 1B shows the tapping-mode AFM height image of the same sample immersed in water. The image remains featureless. The roughness values for the image in Figure 1B are R = 0.23 nm and R_{max} = 2.0 nm. These values are very close to those for the height image corresponding to the sample in air. Thus, with a homogenous PMMA surface, the surface topology remains unchanged in water.

A homogenous PS surface gives a contact angle value of ~97^{o} with water, which indicates that a PS surface is hydrophobic in nature.[30] Figure 1C shows the contact-mode AFM height image of a PS surface in air. The image is featureless without any discernable spatial structure. The roughness values for the image are R = 0.13 nm and R_{max} = 0.86 nm. Figure 1D shows the cross-sectional views along the two lines drawn in Figure 1C.

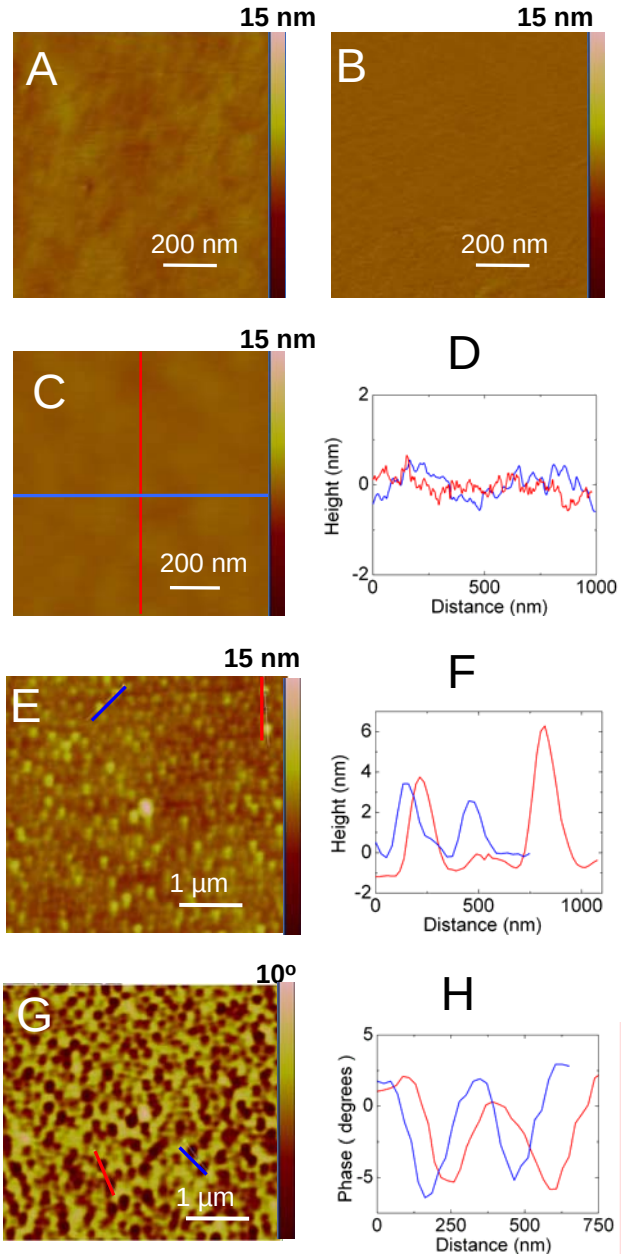

Figure 1. Results from AFM study of homogenous PS and PMMA surfaces: (A) contact-mode AFM height image of PMMA surface in air, (B) tapping-mode AFM height image of PMMA surface in water, (C) contact-mode AFM height image of PS surface in air, (D) cross-sectional views along the lines drawn in Figure 1C, (E) tapping-mode AFM height image of PS surface in water (F) cross-sectional views along the lines drawn in Figure 1E, (G) tapping-mode AFM phase image of PS surface in water, (H) cross-sectional views along the lines drawn in Figure 1G.

The height profile oscillates with an amplitude of less than one nanometer. Figure 1E and 1G show the tapping-mode AFM height and phase images of the same sample in water. In contrast to observations with the PMMA surface, these images are markedly different to those taken with the sample in air. We observe randomly-distributed domains in both the phase as well as height images suggesting a significant difference in material properties at these spots as compared to other locations.[32] At the locations of these features, a larger shift in phase was observed as compared to shift in phase at the locations of any contaminants present on the surface. From this observation, we conclude that these features are 'soft' i.e. deformable in nature. A softer material leads to a larger contact area, which consequently leads to an increase in the duration of tip-sample contact, resulting in a greater phase shift, as compared to a harder material.[33] The roughness values for the height image in this case are R = 1.1 nm and R_{max} = 12 nm. These values are an order of magnitude higher than the values corresponding to the height image of the same surface measured in air. The height and width of the features are found to be 6.0±2.5 nm and (1.6±0.4)×10^2 nm respectively. Further, we see a smooth and symmetric variation in the height and phase profiles along the cross-sections of most of the features (Figure 1F and 1H). The phase profile shows a systematic drop in phase angle from rim to center, which supports the presence of extended gas bubbles that respond with varying compressibility as the tip probes their surfaces.[5] Figure 2A shows an AFM scan over a larger surface area (100 μm^2) of another PS sample under the same conditions as above. We observe the features to be uniformly distributed all over the surface and not localized to a small region. Since the same AFM tip was used in the experiments with hydrophilic substrates (on which no nanobubbles formed) and hydrophobic substrates (on which nanobubbles were present), we believe that nanobubbles are unlikely to be induced by the probe and that they pre-exist on the hydrophobic polystyrene surface. As noted elsewhere,[1] an untreated silicon nitride tip, which was used for imaging in the present study, is hydrophilic and is unlikely to induce bubbles. Presence of nanobubbles in the complete absence of any oscillating AFM tip as shown elsewhere[6] further supports this idea that neither the AFM tip itself nor its oscillation is responsible for the formation of nanobubbles.

In further support of these features being soft air-filled nanobubbles and not polymeric contaminants as speculated in a recent study,[34] we observed a significant effect of variation in tapping force on the morphology of these features (Figure 2). Figure 2A shows the tapping-mode AFM height image of a PS surface in water taken with a 0.9 V amplitude setpoint voltage; the amplitude setpoint voltage determines how much force is applied when the tip taps the surface of the sample. Figure 2A shows uniformly distributed nanobubbles. The sample was then scanned once with a lower setpoint voltage (higher tapping force[31]) followed by scanning again with 0.9 V setpoint voltage. Figure 2B shows the image obtained from this second scanning. The image is markedly different from Figure 2A and shows that large, but less-frequent, features are now present on the surface. These larger features are formed, in our opinion, due to coalescence of smaller bubbles upon being displaced from their original locations. Upon scanning once with a still lower setpoint voltage (0.4 V) followed by scanning with 0.9V setpoint

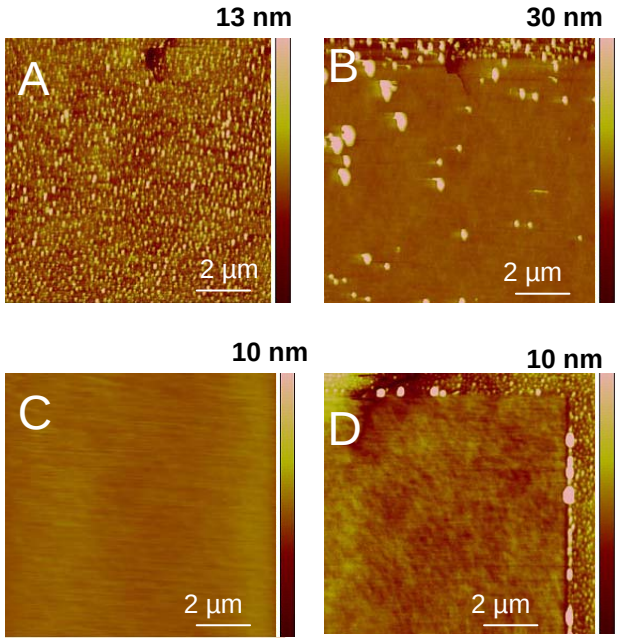

Figure 2. Tapping-mode AFM height images of PS in water (all images taken with a fixed setpoint voltage value of 0.9 V): (A) initial image, (B) after first scanning the surface once at a lower setpoint voltage of 0.6 V (corresponding to a higher tapping force), (C) after scanning the surface once at 0.4 V, (D) at a slightly displaced location after a pause of ~20 minutes.

voltage, the image becomes featureless (Figure 2C) suggesting that, upon much harder tapping, bubbles can be completely scraped off the surface. At this point, the tip was disengaged, and scanning was stopped. After an elapsed period of a few minutes, the tip was re-engaged. Figure 2D shows the image at a slightly displaced location from the previous spot on the surface. The area which was scanned earlier still remains featureless while the region around the periphery of the scanned area shows features similar to those observed in Figure 2A. From the results in Figure 2, we can conclude that the features observed for PS immersed in water are soft air-filled nanobubbles that can be easily manipulated by the AFM tip.

From experiments with homogenous PS and PMMA surfaces, we conclude that, while PMMA surfaces show no change in topology when immersed in water, PS surfaces show presence of nanobubbles with height and width 6.0±2.5 nm and (1.6±0.4)×10^2 nm, respectively. Block copolymer self-assembly was then used to prepare nanopatterned surfaces.[26, 27] Details of the method of preparation are discussed in the Supporting Information.

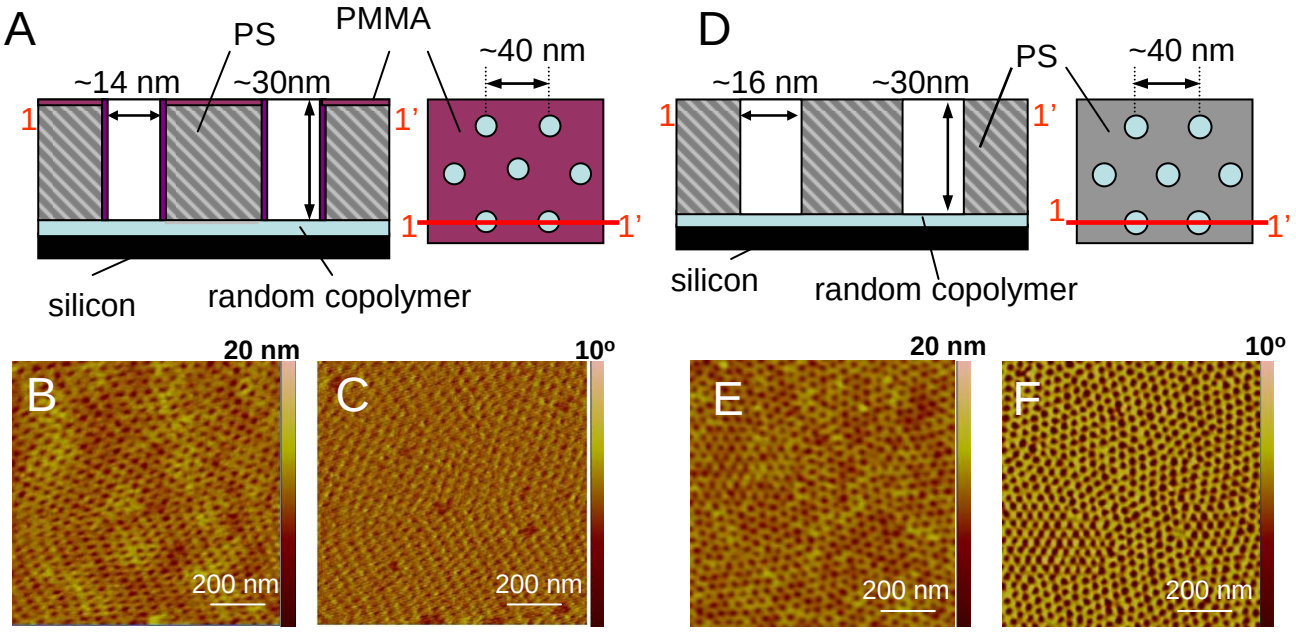

Figure 3. Results with nanopatterned surfaces prepared using block copolymer self-assembly. Patterned PMMA sample: (A) schematic diagram, (B) tapping-mode AFM height image with sample in water, (C) tapping-mode AFM phase image with sample in water. Patterned PS sample: (D) schematic diagram, (E) tapping-mode AFM height image with sample in water, (F) tapping-mode AFM phase image with sample in water.

The first set of nanopatterned samples discussed here consists of patterned PMMA surfaces. Figure 3A shows a schematic diagram of the surface topology of these samples. The surface consists of a regular pattern of pits (spatial period of ~40 nm) in a continuous PMMA matrix, which covers the PS template. The diameter of the pits is ~14 nm whereas the depth of the pits is ~30 nm. The exposed surface at the base of the pits is crosslinked random copolymer brush on silicon wafer. Figure 3B and 3C show the tapping-mode AFM height and phase images of the patterned PMMA sample in water. Besides the regular pattern of pits, there is no evidence of any other feature on the surface. The roughness values from Figure 3B (R = 1.3 nm; R_{max} = 11 nm) are similar to those corresponding to the in-air images (R = 1.2 nm; R_{max} = 10 nm). These values of R_{max} suggest that the vertical distance between the highest and the lowest points in the images is ~10 nm, which is much less than the depth of the pits (~30 nm), measured with ellipsometry prior to removal of PMMA. The AFM tip is not expected to enter the pit completely, since the radius of the end of the tip (~15 nm) is approximately equal to diameter of the pits (~14 nm). Since we already know from experiments with homogenous PMMA surface that PMMA is hydrophilic enough for nanobubbles not to form, the absence of nanobubbles in the case of patterned PMMA sample immersed in water is consistent with rest of the observations.

The second set of patterned samples discussed here consists of patterned PS surfaces. Block copolymer self-assembly was used to prepare these surfaces (See Supporting Information). Figure 3D shows a schematic diagram of the topology of the sample surface. The surface consists of a regular pattern of pits in a PS matrix with a spatial period of ~40 nm. The dimensions are very similar to those of the patterned PMMA surface in Figure 3A; the depth and width of the pits are ~30 nm and ~16 nm, respectively. Since we have already demonstrated that a smooth PS surface immersed in water is hydrophobic enough to support nanobubbles, we may expect this surface to support nanobubbles in water. Figure 3E and 3F show the tapping-mode AFM height and phase images of the sample in water. Contrary to our hypothesis, there appears to be no trace of nanobubbles anywhere in the images. The roughness values (R = 1.1 nm; R_{max} = 9.7 nm) are found to be similar to those for the images taken with

the same sample in air (R = 1.1 nm; R_{max} = 9.8 nm). The absence of nanobubbles on these patterned PS surfaces is a consequence of the observation that the width of a typical nanobubble that develops spontaneously on a flat PS surface is ~100–200 nm, much larger than the available length of polystyrene between any two pits on the patterned surface and, consequently, nucleation is stymied. Thus, in the case of patterned samples, besides the hydrophobicity of the surface, the dimensions of the hydrophobic domains are also an important factor in governing the spontaneous development of nanobubbles.

In order to generate nanobubbles at desired locations, we prepared patterned surfaces with larger-sized hydrophobic domains. With block copolymer self-assembly, preparing large domains was found to be difficult because of the limited mobility of block copolymer with higher molecular weight. To circumvent this problem, we adopted a polymer transfer printing method[28, 29] to prepare a surface with a regular pattern of PS dots on a hydrophilic substrate having a contact angle of ~25^{o} with water (See Supporting Information). Figure 4A shows a schematic diagram of the surface topology, which consists of a regular pattern of PS dots (pitch ~3 μm) in a hydrophilic polyelectrolyte multilayer [poly-(diallyldimethyl ammonium chloride) (PDAC)/poly (styrene-4-sulphonate)]$_{5.5}$ matrix. The height and diameter of the dots are ~10–30 nm and ~500 nm, respectively. Figure 4B shows the contact-mode AFM height image of the sample in air. We see regularly arranged dot structures with diameter ~500 nm and height ~10–30 nm in a featureless background with roughness values of R = 0.36 nm and R_{max} = 1.8 nm (Figure 4B, C and D). Figure 4E shows the tapping-mode AFM height image when the same sample is immersed in water. While there is no difference in the topography of the background between the height images in Figure 4B and Figure 4E, we see a significant difference in topography at the locations of the PS dots in the two images. When the sample is immersed in water, we observe multiple circular-shaped features appearing together in the height and phase images only at the PS dots (Figure 4E, F and H). The height profile across a dot (Figure 4F), unlike that in Figure 4D, shows multiple individual peaks corresponding to protuberances in the shapes of spherical caps rather than a single peak corresponding

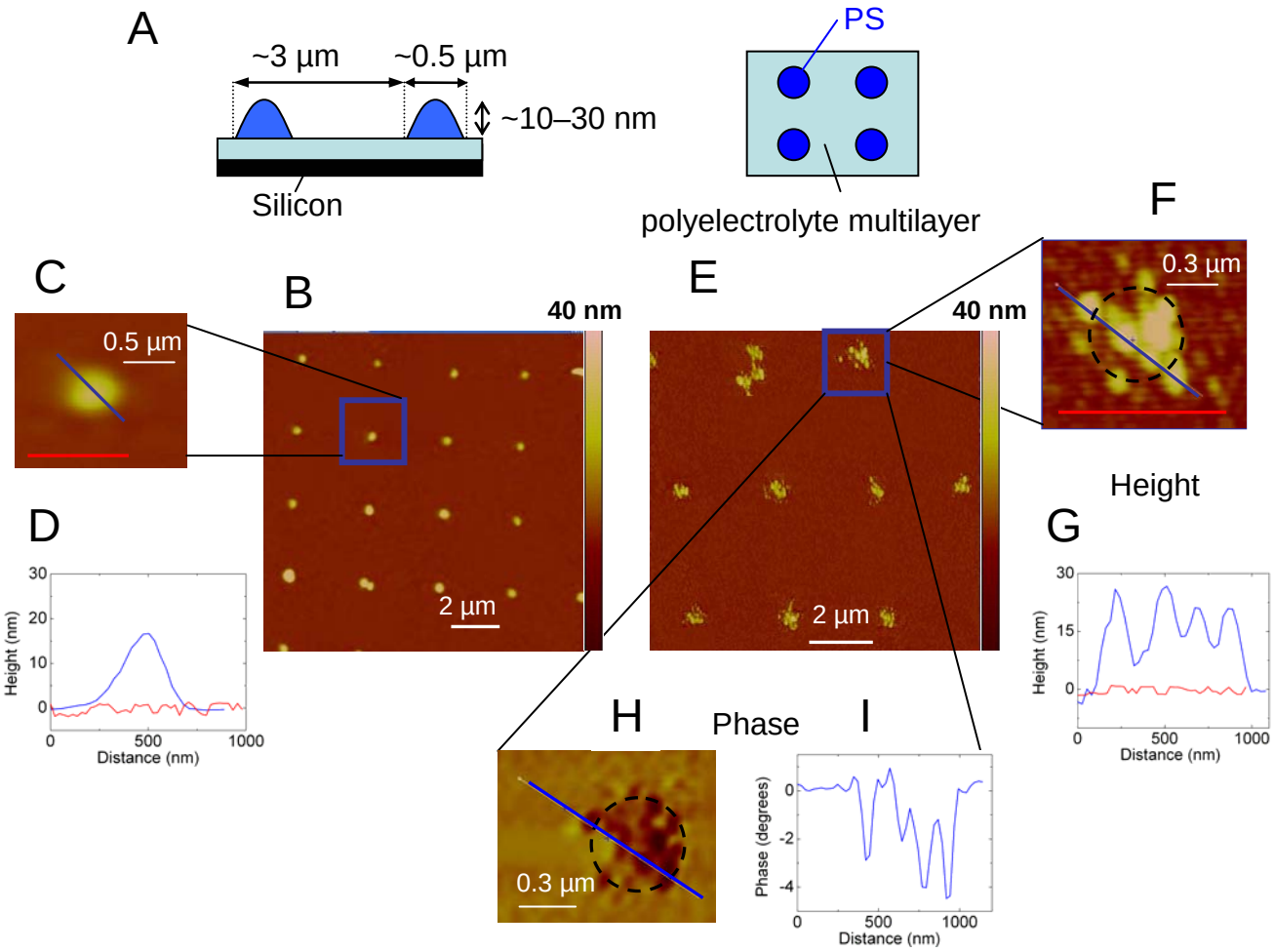

Figure 4. Results with nanopatterned sample prepared using polymer transfer printing. (A) a schematic diagram of the topology of the surface (not to scale), (B) contact-mode AFM height image of sample in air, (C) zoomed image of one of the dots in Figure 4B. (D) cross-sectional views along the lines in Figure 4C, (E) tapping-mode AFM height image with sample in water. (F) zoomed height image of one of the dots in Figure 4E, (G) cross-sectional views along the lines in Figure 4F, (H) zoomed phase image of one of the dots in Figure 4E, (G) cross-sectional view along the line drawn in Figure 4H.

to the dot. The height and width of these individual protuberances, after removal of the contribution from the PS dots, are ~5–15 nm and ~100–200 nm, respectively. These values are similar to the dimensions of nanobubbles observed on homogenous PS surfaces. The significant change in the phase of these features that is observed at each of the PS dots is consistent with our earlier results, in which a

similar phase variation for nanobubbles on homogenous PS surfaces was found. Further, we observed a significant effect of tapping force on the morphology of these features during scanning. Upon harder tapping the features shown in Figure 4F and H disappeared. Thus, we can conclude that the observed features that develop on the PS dots are nanobubbles with dimensions similar to the nanobubbles observed on flat PS surfaces.

In conclusion, we have demonstrated that nanobubbles can form on flat hydrophobic (polystyrene) surfaces and not on flat hydrophilic (PMMA) surfaces. Strong experimental evidences have been shown to support the conclusions that nanobubbles form as expected from earlier studies.[1-8] Nanobubbles did not form on patterned PMMA surfaces. However, they also did not form on patterned PS surfaces in which the lateral area of PS available for bubble formation was too small to allow nucleation. By increasing the surface area of nanopatterned PS features to several hundred nanometers, though, spontaneous nanobubble formation was observed to occur on the PS domains but not on the surrounding hydrophilic background surface. Thus, by using heterogeneous surfaces with controlled chemistry and lateral size, the location and number density of nanobubbles can be systematically controlled. The reduction in viscous skin-friction for microscopic flow past nanopatterned surfaces with well-defined surface patterning is presently being studied to investigate the influence of the size and number of nanobubbles on frictional stresses.

Acknowledgment. This research is supported by the National Science Foundation (NSF) under award No. NSF 03-03916 (Nanotechnology and Interdisciplinary Research Team on wetting of surfaces with nanoscale structures). The authors also thank Dr. Nitin Kumar for many stimulating discussions.

Supporting Information Available: Schematic diagrams of method of preparation of patterned surfaces using block copolymer self-assembly and polymer transfer printing techniques are shown in Figure 1S and 2S, respectively. This material is available free of charge via the Internet at http://pubs.acs.org.

References

(1) Tyrrell, J. W. G.; Attard, P. *Langmuir* **2002**, *18*, 160-167.
(2) Tyrrell, J. W. G.; Attard, P. *Phys. Rev. Lett.* **2001**, *8717*, art. no.-176104.
(3) Yang, J. W.; Duan, J. M.; Fornasiero, D.; Ralston, J. *J. Phys. Chem. B* **2003**, *107*, 6139-6147.
(4) Steitz, R.; Gutberlet, T.; Hauss, T.; Klosgen, B.; Krastev, R.; Schemmel, S.; Simonsen, A. C.; Findenegg, G. H. *Langmuir* **2003**, *19*, 2409-2418.
(5) Simonsen, A. C.; Hansen, P. L.; Klosgen, B. *J. Colloid Interface Sci.* **2004**, *273*, 291-299.
(6) Switkes, M.; Ruberti, J. W. *Appl. Phys. Lett.* **2004**, *84*, 4759-4761.
(7) Ishida, N.; Inoue, T.; Miyahara, M.; Higashitani, K. *Langmuir* **2000**, *16*, 6377-6380.
(8) Holmberg, M.; Kuhle, A.; Garnaes, J.; Morch, K. A.; Boisen, A. *Langmuir* **2003**, *19*, 10510-10513.
(9) Attard, P.; Moody, M. P.; Tyrrell, J. W. G. *Physica A* **2002**, *314*, 696-705.
(10) Attard, P. *Langmuir* **1996**, *12*, 1693-1695.
(11) Parker, J. L.; Claesson, P. M. *Langmuir* **1994**, *10*, 635-639.
(12) Pashley, R. M. *J. Phys. Chem. B* **2003**, *107*, 1714-1720.
(13) Thomas, O. C.; Cavicchi, R. E.; Tarlov, M. J. *Langmuir* **2003**, *19*, 6168-6177.
(14) Zbik, M.; Horn, R. G. *Colloid Surf. A-Physicochem. Eng. Asp.* **2003**, *222*, 323-328.
(15) Stockelhuber, K. W.; Radoev, B.; Wenger, A.; Schulze, H. J. *Langmuir* **2004**, *20*, 164-168.
(16) Lauga, E.; Brenner, M. P. *Phys. Rev. E* **2004**, *70*, art. no.-026311.
(17) Cottin-Bizonne, C.; Barrat, J. L.; Bocquet, L.; Charlaix, E. *Nat. Mater.* **2003**, *2*, 237-240.
(18) Zhu, Y. X.; Granick, S. *Phys. Rev. Lett.* **2001**, *8709*, art. no.-096105.
(19) Lou, S. T.; Ouyang, Z. Q.; Zhang, Y.; Li, X. J.; Hu, J.; Li, M. Q.; Yang, F. J. *J. Vac. Sci. Technol. B* **2000**, *18*, 2573-2575.
(20) Lou, S. T.; Gao, J. X.; Xiao, X. D.; Li, X. J.; Li, G. L.; Zhang, Y.; Li, M. Q.; Sun, J. L.; Hu, J. *Chin. Phys.* **2001**, *10*, S108-S110.
(21) Lou, S. T.; Gao, J. X.; Xiao, X. D.; Li, X. J.; Li, G. L.; Zhang, Y.; Li, M. Q.; Sun, J. L.; Li, X. H.; Hu, J. *Mater. Charact.* **2002**, *48*, 211-214.
(22) Zhang, X. H.; Zhang, X. D.; Lou, S. T.; Zhang, Z. X.; Sun, J. L.; Hu, J. *Langmuir* **2004**, *20*, 3813-3815.
(23) Schneemilch, M.; Quirke, N.; Henderson, J. R. *J. Chem. Phys.* **2004**, *120*, 2901-2912.
(24) Quere, D. *Physica A* **2002**, *313*, 32-46.
(25) Lau, K. K. S.; Bico, J.; Teo, K. B. K.; Chhowalla, M.; Amaratunga, G. A. J.; Milne, W. I.; McKinley, G. H.; Gleason, K. K. *Nano Lett.* **2003**, *3*, 1701-1705.
(26) Xu, T.; Stevens, J.; Villa, J. A.; Goldbach, J. T.; Guarini, K. W.; Black, C. T.; Hawker, C. J.; Russell, T. P. *Adv. Functional Mater.* **2003**, *13*, 698-702.
(27) Ryu, D. Y.; Shin, K.; Drockenmuller, E.; Hawker, C. J.; Russell, T. P. *Science* **2005**, *308*, 236-239.
(28) Park, J.; Kim, Y. S.; Hammond, P. T. *Nano Lett.* **2005**, ASAP.
(29) Kim, Y. S.; Baek, S. J.; Hammond, P. T. *Adv. Mater.* **2004**, *16*, 581-584.
(30) Adamson, A. W., *Physical Chemistry of Surfaces* (John Wiley & Sons, New York, 1990).
(31) *Nanoscope Command Reference Manual for Software Version 5.12* (Digital Instruments/Veeco Metrology Group, Inc., 2001).
(32) Tamayo, J.; Garcia, R. *Langmuir* **1996**, *12*, 4430-4435.
(33) Magonov, S. N.; Elings, V.; Whangbo, M. H. *Surf. Sci.* **1997**, *375*, L385-L391.
(34) Evans, D. R.; Craig, V. S. J.; Senden, T. J. *Physica A* **2004**, *339*, 101-105.